The role of chaotic orbits in the determination of power spectra of passive scalars

Thomas M. Antonsen, Jr., Zhencan Fan, Edward Ott, and E. Garcia-Lopez
University of Maryland, College Park, Maryland 20742

(Received 29 June 1995; accepted 23 May 1996)

This paper relates properties of the power spectrum of a passive scalar convected by a chaotic fluid flow to the distribution of finite time Lyapunov exponents. The properties considered include the early time evolution of the power spectrum, the late time exponential decay of the scalar variance, and the wave number dependence of the power spectrum in the presence of a source of scalar variance. Theoretical predictions are tested by comparing full numerical solutions of the relevant partial differential equation to solutions of a model system which includes diffusion and involves integrations along the fluid orbits only. The model system is shown to give results in close agreement with the numerical solutions of the full problem. This suggests the possible general utility of the model equations for a broad range of problems involving passive scalar convection. [S1070-6631(96)01611-X] © *1996 American Institute of Physics.*

I. INTRODUCTION

The properties of scalar quantities (e.g., temperature or the concentration of an impurity) that are passively convected by an incompressible fluid flow have been of interest for many years.[1] The evolution equation for the passive scalar is

$$\frac{d\phi}{dt} = D\nabla^2\phi + S(\mathbf{x},t), \tag{1}$$

where the time derivative in (1) is taken following the motion of the fluid,

$$\frac{d}{dt} = \frac{\partial}{\partial t} + \mathbf{v}(\mathbf{x},t)\frac{\partial}{\partial \mathbf{x}},$$

where $\mathbf{v}(\mathbf{x},t)$ is the fluid velocity. The quantity D represents the microscopic diffusion coefficient for the scalar, and $S(\mathbf{x},t)$ represents a source of the scalar. Here it is assumed that the fluid motion is incompressible, $\nabla\cdot\mathbf{v}(\mathbf{x},t)=0$ and is determined by external dynamics (such as stirring), that the source $S(\mathbf{x},t)$ is prescribed, and that neither the source nor the fluid flow are affected by the scalar ϕ.

In the absence of a source and diffusion, Eq. (1) states that the value of the scalar ϕ is constant in a moving fluid element. The trajectory of the fluid element is given by the equation,

$$\frac{d\boldsymbol{\xi}(\mathbf{x},t)}{dt} = \mathbf{v}(\boldsymbol{\xi},t) \tag{2}$$

with the initial condition

$$\boldsymbol{\xi}(\mathbf{x},t) = \mathbf{x}.$$

Thus, $\boldsymbol{\xi}(\mathbf{x},t)$ is the position at time t of the fluid element which is located at $\mathbf{x}$ at time $t=0$. The properties of the trajectories of the fluid elements can be expected to affect the solutions for the scalar ϕ both when diffusion is negligible ($D=0$) and when it is not. The purpose of this paper is to explore this relationship in the case in which the trajectories given by Eq. (2) are chaotic in the sense that nearby fluid elements diverge exponentially from each other.[1–4]

Specifically, we will explore the relationship of the time evolution of the power spectrum of the passive scalar to the distribution of the finite time Lyapunov exponents of the flow. Previous work along these lines appears in Refs. 2 and 3 which we discuss subsequently.

The power spectrum of the passive scalar is the Fourier transform of the two point correlation function,

$$C(\mathbf{r},t) = \langle \phi(\mathbf{x}+\mathbf{r},t)\,\phi(\mathbf{x},t)\rangle, \tag{3}$$

where the average is taken over the $\mathbf{x}$-domain in which Eq. (1) is solved. The power spectrum $F(k,t)$ is then defined

$$F(k,t) = \int \frac{d^n\mathbf{k}'}{(2\pi)^n}\,\delta(k-|\mathbf{k}'|)\,\overline{C}(\mathbf{k}',t), \tag{4}$$

where

$$\overline{C}(\mathbf{k}',t) = \int d^n\mathbf{r}\,C(\mathbf{r},t)\exp[-i\mathbf{k}'\cdot\mathbf{r}], \tag{5}$$

is the Fourier transform of the correlation function and n is the dimensionality of the domain. The present paper will consider the two dimensional case exclusively.

The chaotic orbits of the flow can be characterized by their finite time Lyapunov exponents. These may be defined as follows. Consider two trajectories which initially are separated by the vector $\mathbf{r}$, $\boldsymbol{\xi}(\mathbf{x}+\mathbf{r},t)$ and $\boldsymbol{\xi}(\mathbf{x},t)$. Considering $\mathbf{r}$ to be a differential vector, the differential separation $\delta\boldsymbol{\xi}(\mathbf{x},t) = \boldsymbol{\xi}(\mathbf{x}+\mathbf{r},t) - \boldsymbol{\xi}(\mathbf{x},t)$ satisfies the linear equation,

$$\frac{d}{dt}\,\delta\boldsymbol{\xi}(x,t) = \delta\boldsymbol{\xi}\cdot\nabla\mathbf{v}(\boldsymbol{\xi}(\mathbf{x},t),t), \tag{6}$$

with initial condition,

$$\delta\boldsymbol{\xi}(x,t) = \mathbf{r}.$$

For chaotic flows the separation $\delta\boldsymbol{\xi}$ typically diverges exponentially in time, and the net rate of exponentiation over the time interval from 0 to t,

$$h(\mathbf{x},t) = \frac{1}{t}\log\frac{|\delta\boldsymbol{\xi}|}{|\mathbf{r}|}, \tag{7}$$

 1070-6631/96/8(11)/3094/11/$10.00 © 1996 American Institute of Physics

Downloaded¬10¬Jul¬2006¬to¬171.64.163.13.¬Redistribution¬subject¬to¬AIP¬license¬or¬copyright,¬see¬http://pof.aip.org/pof/copyright.jsp

is the finite time Lyapunov exponent. Defined in this way, the exponent, h, depends on the orientation of the vector $\mathbf{r}$ and on the initial coordinates, $\mathbf{x}$, as well as on the time, t. In the limit $t\to\infty$ almost every initial condition in a given chaotic region yields the same value of h which is the Lyapunov exponent and is denoted by $\overline{h}$,

$$\overline{h}=\lim_{t\to\infty} h(\mathbf{x},t).$$

For finite times there is a distribution of values of h which may be characterized by a probability distribution $P(h,t)$, where $P(h,t)dh$ is the probability that $h(\mathbf{x},t)$ is between h and $h+dh$, if $\mathbf{x}$ is chosen randomly with uniform probability in the relevant ergodic fluid region. Later in the paper we shall relate various properties of the power spectrum to the probability distribution $P(h,t)$.

To verify our predictions we will compare them with numerical solutions of Eq. (1) for a specific realization of the flow $\mathbf{v}(\mathbf{x},t)$,

$$\mathbf{v}(\mathbf{x},t)=U[\mathbf{e}_x f_1(t)\cos(2\pi y/L+\theta_1(t)) + \mathbf{e}_y f_2(t)\cos(2\pi x/L+\theta_2(t))], \tag{8}$$

which is periodic in x and y with period L. The time dependent functions f_1 and f_2 are defined as follows. Both are periodic with period T,

$$f_1(t)=\begin{cases}1 & 0<t<T/2\\ 0 & T/2\leqslant t<T\end{cases}$$

and

$$f_2(t)=\begin{cases}0 & 0\leqslant t<T/2\\ 1 & T/2\leqslant t<T.\end{cases}$$

The flow $\mathbf{v}$ is in the x direction during the first half of each period and in the y direction during the second half. The angles θ_1 and θ_2 take on different values in each time period. If all the angles θ_1 and θ_2 are set to zero then the phase space flow is periodic in time, and, depending on the initial value of $\mathbf{x}$, solutions of Eq. (2) yield either chaotic or nonchaotic orbits. If the angles θ_1 and θ_2 are constant in each period $nT\leqslant t\leqslant(M+1)T$, but vary randomly from period to period, then all the orbits are chaotic (i.e., $h>0$). Examples of each case will be shown. The evolution of a passive scalar in this flow has also been considered in Ref. 4.

To solve Eq. (7) with the given flow velocity we assume the scalar has the same spatial periodicity as the flow and express the scalar ϕ in terms of its Fourier series

$$\phi(x,y)=\sum_{mn}\phi_{mn}(t)\exp\left[\frac{2\pi i}{L}(nx+my)\right].$$

We then obtain the following evolution equation for $\phi_{nm}(t)$,

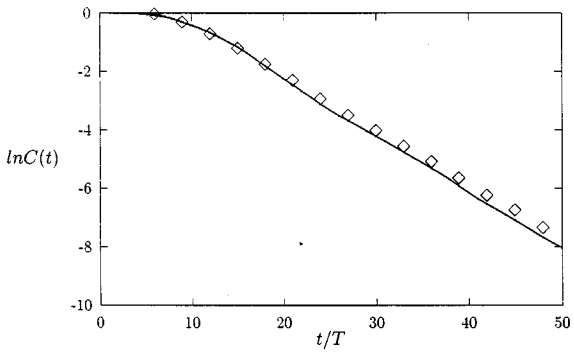

FIG. 1. A plot of $\ln C(t)$ versus t/T. The solid curve is the result of a full numerical solution (Fourier) of Eq. (1). The diamonds correspond to the RKS model introduced in Sec. II.

$$\dot{\phi}_{nm}(t)+\frac{i\pi U}{L}\{nf_1(t)[\exp(i\theta_1)\phi_{nm-1}+\exp(-i\theta_1)\phi_{nm+1}] + mf_2(t)[\exp(i\theta_2)\phi_{n-1\,m}+\exp(-i\theta_2)\phi_{n+1\,m}]\} = -\left(\frac{2\pi}{L}\right)^2 D(m^2+n^2)\phi_{nm}+S_{nm}, \tag{9}$$

where S_{nm} is the Fourier coefficient of the source S. (Note that (9) involves coupling of (n,m) only to the neighboring Fourier modes $(n,m\pm1)$ and $(n\pm1,m)$.) Equation (9) is integrated numerically for a finite set of values of n,m. The power spectrum $F(k,t)$ can be related to the Fourier amplitudes ϕ_{nm} by

$$F(k,t)=\sum_{nm}|\phi_{nm}|^2\delta(k-k_{nm}), \tag{10}$$

where

$$k_{nm}=\frac{2\pi}{L}(n^2+m^2)^{1/2}.$$

The results of a sample run are shown in Fig. 1 where we have plotted the log of the scalar variance $C(t)$,

$$C(t)=\int_0^L\frac{dxdy}{L^2}\phi^2(x,y,t)=\sum_{nm}|\phi_{nm}(t)|^2=\int_0^\infty F(k,t)dk,$$

versus time, normalized to the period T. The parameters for this run were $S_{nm}=0$, $e=UT/L=0.5$, $q=(2\pi/L)^2DT=0.00000125$, $|m|$, $|n|\leqslant500$, and $\theta_1(t)$ and $\theta_2(t)$ were selected randomly in each time interval with uniform probability distribution between 0 and 2π. Initially, $\phi(x,y,0)=2\{\cos[2\pi(x-y)/L]-\cos[2\pi(x+y)/L]\}$. Figure 1 shows that there is an initial period of time lasting about 8 periods during which the scalar variance is constant, and then a transition to a late time behavior where the scalar variance decays exponentially in time at a fixed rate. The rate of change of scalar variance can be derived from Eq. (1) or Eq. (9),

$$\frac{dC(t)}{dt}=-2q\sum_{nm}(n^2+m^2)|\phi_{nm}|^2. \tag{11}$$

Downloaded¬10¬Jul¬2006¬to¬171.64.163.13.¬Redistribution¬subject¬to¬AIP¬license¬or¬copyright,¬see¬http://pof.aip.org/pof/copyright.jsp

During the initial period of time the Fourier spectrum $|\phi_{nm}|^2$ is concentrated at sufficiently small wave numbers such that, owing to the small value of diffusion ($q=0.00000125$), dissipation of the variance is negligible. We refer to this phase as the initial transient and we will discuss its properties in Sec. II. Later, the variance damps exponentially as if the scalar has formed an eigenfunction with a fixed rate of decay. This phase has been studied recently by Pierrehumbert.[4] We will relate the properties of the scalar to the chaotic orbits during this late time phase in Sec. III. In particular, we show that the power spectrum $F(k,t)$ factorizes into the product $\exp(-\nu t)M(\sqrt{D}k)$ where the function M and the decay rate ν depend only on the chaotic dynamics. Section IV will discuss the modifications to our results that occur when the phase space has both chaotic and integrable trajectories. Finally, Sec. V will relate the behavior of the power spectrum of the scalar during the initial transient to that predicted by Batchelor's law[5] which applies to cases in which a source is present.

Throughout we will present detailed comparison between the solutions of the full partial differential equation (Eq. (1)), with a model system (Eqs. (15) and (21)), which includes diffusion and is based on integration along fluid element orbits. Solution of the model system is much faster and more economical as compared to solution of the full problem, yet the model system yields results in close agreement with those for the full problem. This suggests the general utility of the model system for passive scalar problems (in addition, to those treated specifically in this paper).

II. INITIAL TRANSIENT

During the first eight periods of the simulation in Fig. 1 the scalar variance is nearly constant implying that diffusion may be neglected. We have considered this case in our previous work[2] and have shown that the power spectrum $F(k,t)$ can be related to the distribution of finite time Lyapunov exponents by

$$F(k,t)\cong(kt)^{-1}P\left[t^{-1}\ln\frac{k}{k_0},t\right], \tag{12}$$

where k_0 is the magnitude of the initial wave vector of the scalar and $P(h,t)$ is the probability density function for finite time Lyapunov exponents discussed previously. We now rederive, heuristically, this expression by introducing a model which we term the reduced k spectrum model (RKS). This model follows very closely the previous analysis of both Batchelor and Kraichnan.[5] A more rigorous derivation of this model is contained in the Appendix.

In the absence of diffusion, the value of the scalar is constant following a fluid trajectory. Thus, if we consider two infinitesimally separated trajectories we have

$$\phi(\boldsymbol{\xi}(\mathbf{x}+\mathbf{r},t),t)-\phi(\boldsymbol{\xi}(\mathbf{x},t),t)$$
$$=\boldsymbol{\delta\xi}(\mathbf{x},t)\cdot\nabla\phi(\boldsymbol{\xi}(\mathbf{x},t),t)=\text{const.}$$

This implies

$$\frac{d}{dt}\delta\boldsymbol{\xi}\cdot\nabla\phi=0. \tag{13}$$

Now imagine that we initially divide the fluid into many small areas. We consider the case in which the initial condition is in the form of a modulated sinusoidal function of $\mathbf{x}$; that is, $\phi(\mathbf{x},0)=A(\mathbf{x})\sin(\int^{\mathbf{x}}\mathbf{k}_i(\mathbf{x})d\mathbf{x}+\theta(\mathbf{x}))$ where $\mathbf{k}_i(\mathbf{x})$, $A(\mathbf{x})$, and $\theta(\mathbf{x})$ vary on the scale of the flow which is much larger than $|\mathbf{k}_i|^{-1}$. To each area we can then assign a mean wave vector $\mathbf{k}$. As the scalar is advected by the flow the mean value of the scalar in each evolving fluid element is constant. Equation (13) then suggests that the wave number evolves according to

$$\frac{d}{dt}\delta\boldsymbol{\xi}\cdot\mathbf{k}=0. \tag{14}$$

Using Eqs. (6) and (14) the evolution equation for $\mathbf{k}$ is

$$\frac{d}{dt}\mathbf{k}=-(\nabla\mathbf{v})\cdot\mathbf{k}. \tag{15}$$

In two dimensions the differential separation equation, Eq. (6), will have two linearly independent solutions $\delta\boldsymbol{\xi}_1$ and $\delta\boldsymbol{\xi}_2$. Due to the incompressible nature of the flow the area of the parallelogram defined by $\delta\boldsymbol{\xi}_1$ and $\delta\boldsymbol{\xi}_2$ is constant $J=\hat{z}\cdot\delta\boldsymbol{\xi}_1\times\delta\boldsymbol{\xi}_2$,

$$\frac{d}{dt}J=0. \tag{16}$$

Generally, $\delta\boldsymbol{\xi}_1$ and $\delta\boldsymbol{\xi}_2$ can be chosen such that if $\delta\boldsymbol{\xi}_1$ is growing exponentially $\delta\boldsymbol{\xi}_2$ is decreasing exponentially. Comparing (14) and (15) we note that the solution for $\mathbf{k}$ may be written

$$\mathbf{k}(t)=J^{-1}[(\mathbf{k}(0)\cdot\delta\boldsymbol{\xi}_2(0))\hat{z}\times\delta\boldsymbol{\xi}_1(t)$$
$$-(\mathbf{k}(0)\cdot\delta\boldsymbol{\xi}_1(0))\hat{z}\times\delta\boldsymbol{\xi}_2(t)]. \tag{17}$$

Thus, $\mathbf{k}(t)$, like the differential displacement, will consist of an exponentially growing and an exponentially decreasing component. The amount of each component depends on the orientation of the initial wave vector, $\mathbf{k}(0)$, relative to the initial displacements $\delta\boldsymbol{\xi}_1(0)$ and $\delta\boldsymbol{\xi}_2(0)$. The exponentially growing solution for the wave vector $\mathbf{k}(t)$ is proportional to the component of the initial wave vector in the contracting direction, $\delta\boldsymbol{\xi}_2(0)$. This is represented by the first term in the sum of Eq. (17).

Under the present model, the power spectrum can be written

$$F(k,t)=\sum_{\ell}\omega_{\ell}(t)\,\delta(k-|\mathbf{k}_{\ell}(t)|), \tag{18}$$

where $\omega_{\ell}(t)$ is the variance contained in the ℓth initial area (which does not vary in the absence of diffusion), and $\mathbf{k}_{\ell}(t)$ is the time evolving wave vector for the fluid trajectory followed by the ℓth element of area. To obtain Eq. (12) we note that for large time

$$k_{\ell}(t)\sim k_0\exp(h_{\ell}t),$$

where h_{ℓ} is the finite time Lyapunov exponent corresponding to the ℓth initial condition. We then replace the weighted sum over initial conditions with an integration over the probability function for finite time Lyapunov exponents

Downloaded¬10¬Jul¬2006¬to¬171.64.163.13.¬Redistribution¬subject¬to¬AIP¬license¬or¬copyright,¬see¬http://pof.aip.org/pof/copyright.jsp

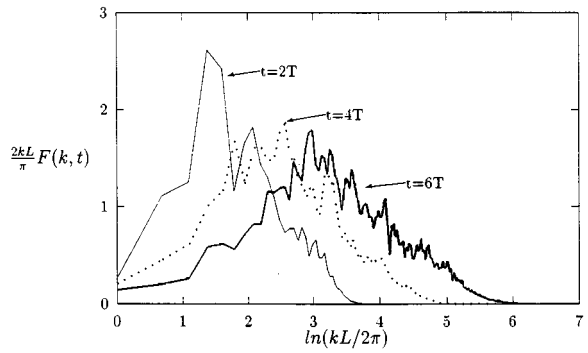

FIG. 2. Power spectra $F(k,t)$ for three times, $t=2T$, $4T$, and $6T$, obtained from the Fourier code.

$$F(k,t)=\int dhP(h,t)\delta[k-k_0\exp(ht)],$$

where we have assumed for simplicity that the initial weights, $\omega_{\not}$ and wave numbers $|k_{\not}\cos|=k_0$ are the same for all elements. Performing the integral over h results in (12).

To test this prediction for the power spectrum we compare a numerically generated histogram of $F(k,t)$ obtained from Eq. (10) and the numerical results of the Fourier amplitude code with one obtained from Eq. (18) by solving the orbit and wave vector equations, Eqs. (2) and (15) for an ensemble of 200×200 trajectories initially distributed uniformly on the simulation area. In this case, the initial condition is taken to be $\phi(x,y,0)=2\{\cos[4\pi(x-y)/L]-\cos[4\pi(x+y)/L]\}$. For the particular realization of the flow under consideration, Eq. (8), the solutions of Eqs. (2) and (15) can be expressed as two dimensional maps,

$$x_{n+1}=x_n+\frac{1}{2}UT\cos\left(\frac{2\pi}{L}y_n+\theta_{1n}\right),$$

$$y_{n+1}=y_n+\frac{1}{2}UT\cos\left(\frac{2\pi}{L}x_{n+1}+\theta_{2n}\right)$$

and

$$k_{y,n+1}=k_{y,n}+\frac{\pi UT}{L}\sin\left(\frac{2\pi}{L}y_n+\theta_{1n}\right)k_{x,n},$$

$$k_{x,n+1}=k_{x,n}+\frac{\pi UT}{L}\sin\left(\frac{2\pi}{L}x_n+\theta_{2n}\right)k_{y,n+1}.$$

The results of the Fourier amplitude code are displayed in Fig. 2 where a histogram of $F(k,t)$ is plotted versus $\ln k$ for times $t=2T$, $4T$, and $6T$. As can be seen, the power spectrum has the form of a pulse which moves to higher values of $\ln k$ and spreads out as time progresses. This is the behavior predicted previously based on Eq. (12). The peak of the pulse moves with a velocity equal to the Lyapunov exponent h and the spreading of the pulse is due to the distribution of finite time Lyapunov exponents.

A comparison with the results of the orbit code (Eqs. (15) and (18)) is shown in Fig. 3 where the histograms of

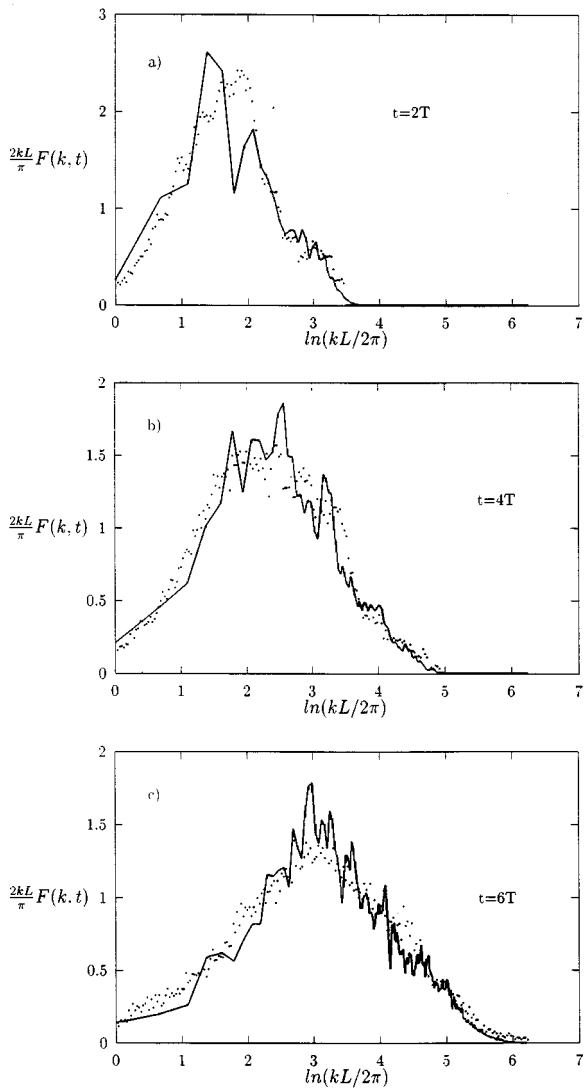

FIG. 3. Comparison of results from the Fourier code (solid curves) with the results from the RKS model (dots) for (a) $t=2T$, (b) $t=4T$, and (c) $t=6T$.

$F(k,t)$ from the two codes are plotted on the same axes. As can be seen both codes predict the same pulse-like behavior of the power spectrum.

Grey scale intensity plots of the scalar from the full numerical solution at four different times are displayed in Fig. 4. Recent work by ourselves and others[2,3,6] has focused on another quantity of interest, namely, the fractal dimension of the measure of the gradient of the scalar. In particular, in Ref. 3 we defined a measure μ of a region of space s based on the distribution of $|\nabla\phi|^\gamma$,

$$\mu(s,t,\gamma)=\frac{\int_s|\nabla\phi|^\gamma d^nx}{\int_{V_0}|\nabla\phi|^\gamma d^nx}, \tag{19}$$

where V_0 is a reference domain in which (1) is satisfied and s is a subset of this domain. The situation was considered in which the flow was smooth on large scales, meaning that the smallest flow scale is much larger than the scales which develop in the variation of the passive scalar $\phi(\mathbf{x},t)$. Moreover, the flow was assumed to be chaotic and ergodic in V_0.

Downloaded¬10¬Jul¬2006¬to¬171.64.163.13.¬Redistribution¬subject¬to¬AIP¬license¬or¬copyright,¬see¬http://pof.aip.org/pof/copyright.jsp

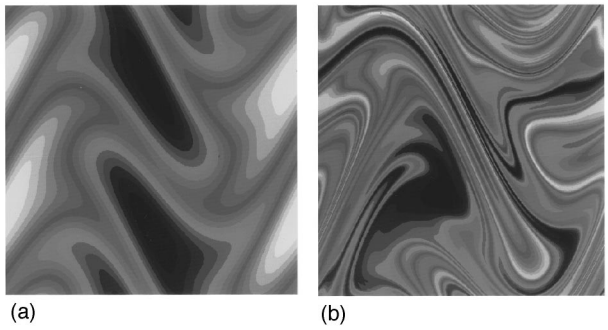

FIG. 4. Grey scale intensity plot of the scalar for (a) $t=1T$, (b) $t=5T$. Here the white indicates the highest values and black the lowest values.

For the initial-value problem it was found[2] that in the case of small diffusivity the measure μ exhibited fractal properties over some time interval determined by the diffusivity and the flow. To understand this, first consider the case where there is no diffusion $D\equiv 0$. Then, as time increases, $\phi(\mathbf{x},t)$ develops finer and finer scale variations, and the regions of largest $|\nabla\phi|$ occupy a smaller and smaller fraction of space. This fraction approaches zero as $t\to\infty$, and in this limit, in an appropriate sense, the region of largest $|\nabla\phi|$ approaches a fractal set. At any large finite time, the region of largest $|\nabla\phi|$ will be approximately fractal in that, when viewed with finite spatial resolution [larger than some appropriate characteristic scale of the region of large $|\nabla\phi|$ (this length scale decreases with time)], the region looks fractal. If $D\neq 0$, but is very small, then the preceding considerations apply up to some finite time t_D at which the characteristic scale mentioned above becomes so small that diffusion cannot be neglected. This time corresponds to the initial seven periods in the present simulations. After this time the measure was shown in Ref. 3 to no longer be fractal. Our current interest is in the intermediate range of times where t is large enough that the measure is approximately fractal, but small enough that diffusion plays no role ($t<t_D$). This behavior of the gradient is illustrated in Fig. 5 where grey scale intensity plots of the measure $\mu(s,t,1)$ are displayed for the same times as in Fig. 4. The measure is constructed by calculating the gradient as a function of position from the full Fourier code (Eq. (9)). The formation of narrow striations with a Cantor set-like structure can be seen in the figure.

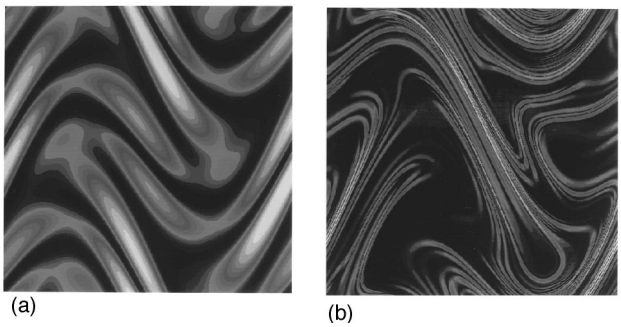

FIG. 5. Grey scale intensity plot of the measure $\mu(s,t,1)$ defined in Eq. (19) for (a) $t=1T$ and (b) $t=5T$.

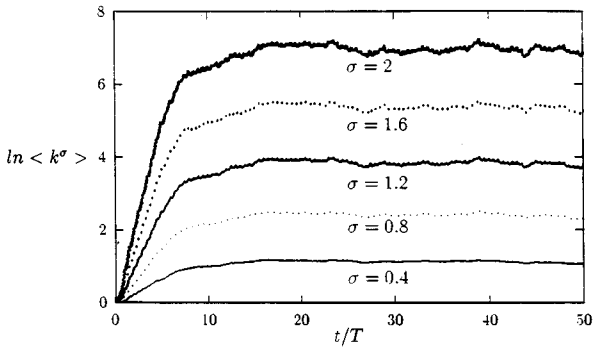

FIG. 6. The logarithm of moments of the power spectrum, $\ln\langle k^{\sigma}\rangle$ versus t/T for $\sigma=2$, 1.6, 1.2, 0.8, and 0.4.

Our previous theoretical work on the power spectrum predicted that the appearance of the multifractal measure μ would be accompanied by the exponential growth of various moments of the power spectrum. In particular, during the initial evolution of the scalar,

$$\langle k^{\sigma}\rangle \sim \exp[\Gamma(\sigma)t],$$

where

$$\langle k^{\sigma}\rangle = \left[\int_0^{\infty} dk F(k,t)k^{\sigma}\right]\left[\int_0^{\infty} dk F(k,t)\right]^{-1}.$$

This behavior is confirmed in Fig. 6 where we plot $\ln\langle k^{\sigma}\rangle$ versus time for five values of σ and $F(k,t)$ from the Fourier code. It can be seen that during the initial 7 periods when diffusion is negligible this quantity grows linearly with time reflecting the constancy of $\Gamma(\sigma)$ during this period. The slope of each curve gives the value of Γ for each σ. These are plotted on Fig. 7. The dependence of Γ on σ is clearly nonlinear. In our previous work it was shown that the multifractal dimension D_q of the measure μ could be obtained from the dependence of Γ on σ.

The spectrum of fractal dimensions D_q (where q is a continuous parameter) characterizes the multifractal properties of the measure μ. Roughly speaking, D_q specifies the scaling of $\langle\langle \mu_{\epsilon}^{(q-1)}\rangle\rangle$ where μ_{ϵ} is the measure in a small box of side ϵ and the average $\langle\langle \ldots \rangle\rangle$ is over all boxes and taken

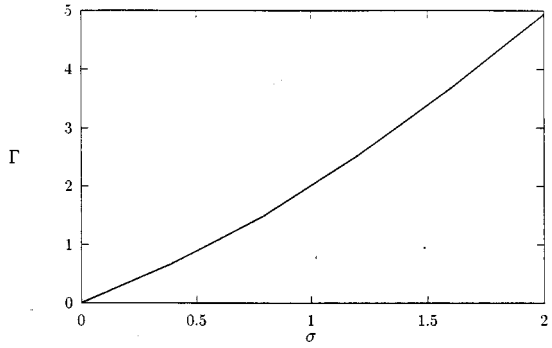

FIG. 7. Growth exponent $\Gamma(\sigma)$ versus σ for the initial transient phase.

Downloaded¬10¬Jul¬2006¬to¬171.64.163.13.¬Redistribution¬subject¬to¬AIP¬license¬or¬copyright,¬see¬http://pof.aip.org/pof/copyright.jsp

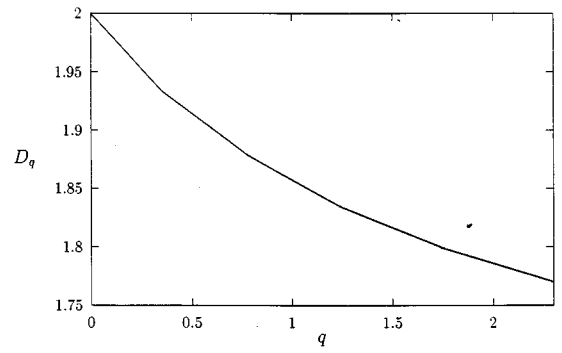

FIG. 8. Predicted dimension D_q of the measure $\mu(s,t,1)$ versus q.

with respect to the measure μ itself. The average defining D_q scales with ϵ as $\langle\langle \mu_\epsilon^{(q-1)} \rangle\rangle \sim \epsilon^{(q-1)D_q}$ for small ϵ (e.g., see Grassberger *et al.*[7] and references therein). The relationship between D_q and $\Gamma(\sigma)$ was shown[2] to be

$$\sigma=(q-1)(D_q-2)+q, \tag{20}$$

where $q=\Gamma(\sigma)/\Gamma(1)$. Using Eq. (20) and the result for $\Gamma(\sigma)$ from Fig. 7, D_q versus q is plotted in Fig. 8.

III. LONG TIME DECAY

Figure 1 shows that for $t>20T$ the scalar variance decays exponentially with time at a fixed rate. This decay has been observed and discussed previously by Pierrehumbert.[4] We now show that the rate of decay can be determined from the distribution of finite time Lyapunov exponents, and depends on a small number of orbits where the initial gradient is aligned perpendicular to the contracting direction.

First, we augment our wave vector model introduced in the previous section by allowing the elemental variances ω_ℓ in Eq. (18) to depend on time. These variances will decay at a rate determined by the diffusion coefficient and the local wave vector as the local wave vector increases

$$\frac{d}{dt}\omega_\ell(t)=-2k_\ell^2(t)D\omega_\ell(t),$$

or integrating this

$$\omega_\ell(t)=\omega_\ell(0)\exp\left[-2D\int_0^t k_\ell^2(t')dt'\right]. \tag{21}$$

The time dependence of the total variance is then given by

$$C(t)=\sum_\ell \omega_\ell(t).$$

To verify this, we have computed the weights given by (21) for the same ensemble of orbits discussed in the previous section. The time dependence of $\ln C(t)$ is then plotted on Fig. 1 along with that produced by the full Fourier amplitude code. The predictions are in close agreement. Thus, the long time decay of the variance can be described in terms of the chaotic orbits.

To analytically arrive at a value for the decay rate we need to evaluate $C(t)=\Sigma_\ell \omega_\ell(t)$. From Eq. (21) it is seen that the time behavior of the elemental variances $\omega_\ell(t)$ is determined by the growth of the magnitude of the corresponding wave number $k_\ell(t)$. If one substitutes the approximation $k_\ell(t)\sim k_0\exp(h_\ell t)$, one finds that the weight is constant until a time $t_D\sim\ln(2h/k_0^2D)/(2h)$, and then quickly decays to zero much faster than a simple exponential. Thus, most orbits do not contribute to the long time decay of the variance as their elemental variances have already decayed.

The long time behavior of the variance is determined by orbits for which the simple approximation $k_\ell(t)=k_0\exp(h_\ell t)$ is not adequate. In particular, we note from the more accurate expression (17) that the amplitude of the exponentially growing component of $\mathbf{k}(t)$ is proportional to the cosine of the angle between the initial wave vector $\mathbf{k}(0)$ and the exponentially decaying solution $\delta\boldsymbol{\xi}_2(0)$. Thus, if the initial wave vector is at right angles to the decaying solution (the contracting direction), $\mathbf{k}(t)$ will not grow exponentially in time. This effect can be treated in the following way. We write

$$k_\ell(t)\sim k_0\cos\phi_\ell\exp[h_\ell t]$$

where $\cos\phi_\ell$ accounts for the orientation of the initial $\mathbf{k}_\ell$ with respect to $\delta\boldsymbol{\xi}_2(0)$. We then assume that for the ensemble of orbits, the angles ϕ_ℓ are randomly distributed, and independent of the finite time Lyapunov exponents, h_ℓ. We then replace the sum over elemental variances with integrals over the angle ϕ and the finite time Lyapunov exponent h

$$C(t)=\int_0^\infty dhP(h,t)\int_0^{2\pi}\frac{d\phi}{2\pi}\times\exp\left[-\frac{k_0^2D\cos^2\phi\exp[2ht]}{h}\right].$$

As discussed, for late times the factor $k_0^2D\exp[2ht]/h$ is large, and the dominant contribution to the integral comes from small values of $\cos\phi$. Expanding about $\phi=\pm\pi/2$ and integrating gives

$$C(t)=\left(\frac{2}{\pi k_0^2D}\right)^{1/2}\int_0^\infty h^{1/2}dhP(h,t)\exp[-ht].$$

We now perform the h integration by noting that the $P(h,t)$ distribution is well approximated as

$$P(h,t)=\left[\frac{tG''(h)}{2\pi}\right]^{1/2}\exp[-tG(h)], \tag{22}$$

where $G(h)=G'(h)=0$ (the prime denotes differentiation with respect to h). This distribution is the same as that which results from the multiplication of many random numbers. Equation (22) is the so-called ''large deviation'' result for a random variable which is the average of many independent, identically distributed variables, and gives $P(h,t)$ (a function of the two variables h and t) in terms of a function of one variable, $G(h)$. The usual Gaussian result is obtained by expanding $G(h)$ about its minimum $h=\bar{h}$, $G(h)\cong 1/2\,G''(\bar{h})\times(h-\bar{h})^2$. The Gaussian result is good if the range of h of interest is limited such that the numbers of standard deviations from $\bar{h}$ is not too large [the standard deviation of the Gaussian is $(G''n)^{-1/2}$]. In doing the above integral for $C(t)$, however, the main contribution comes from a saddle

Downloaded¬10¬Jul¬2006¬to¬171.64.163.13.¬Redistribution¬subject¬to¬AIP¬license¬or¬copyright,¬see¬http://pof.aip.org/pof/copyright.jsp

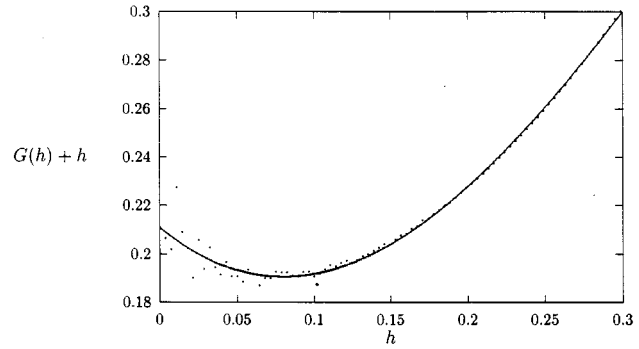

FIG. 9. Data for $G(h)+h$ at time $t=50T$ (dots) and a third order polynomial fit versus h.

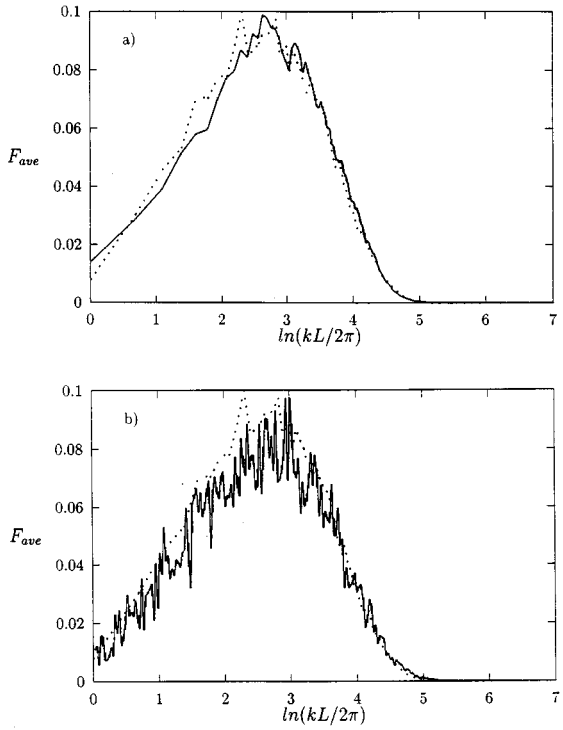

FIG. 10. (a) The quantity $F(k,t)/\int dkF(k,t)$ computed from the Fourier code averaged over time $11\leqslant t/T\leqslant 20$ (solid curve) and averaged over time $21\leqslant t\leqslant 30$ (dotted curve). (b) The average of $F(k,t)$ averaged over time $20\leqslant t\leqslant 30$ using the Fourier code (dotted curve) and using the orbit code (solid curve). The slight systematic off-set between the two curves in (b) is due to a difference in $\int F(k,t)dk$ from the orbit code as compared to the Fourier code. This difference is small considering that the overall amplitude decays by a factor between $t=0$ and $t=25$.

point $h=h_c$ (which is independent of n). Consequently the number of standard deviations between h and h_c diverges like $n^{1/2}$ as n increases, and the more accurate large deviation form (22) is necessary. The form (22) has been numerically verified and used for cases where there are no KAM (Kolmogorov, Arnold, and Moser) surfaces[7–11] [this occurs, in particular, for the situation in which the time dependence of the flow is nonperiodic (e.g., the Eulerian velocity $\mathbf{v}(\mathbf{x},t)$ is itself temporally chaotic)]. As in Refs. 7–11 we find very good agreement with (22) for our flow given by (8). Also, Eq. (22) is expected to apply for time-periodic flows, $\mathbf{v}(\mathbf{x},t)=\mathbf{v}(\mathbf{x},t+T)$, if KAM surfaces are essentially absent (e.g., the standard map at large nonlinearity parameter). In the presence of KAM surfaces bounding the relevant chaotic region, as typically arises for two-dimensional time-periodic flows, there are important modifications of Eq. (22). These modifications[8,9] are due to the ''stickiness'' of KAM surfaces, leading orbits near KAM surfaces to remain near them for long times.

In the absence of KAM surfaces the integration over h may be carried out using the method of steepest descent. The essential result is that

$$C(t)\sim\exp(-\nu t),$$

where

$$\nu=(h_c+G(h_c)), \tag{23}$$

and h_c is determined by

$$1+G'(h_c)=0.$$

Note that $G'(h)\gtrless 0$ when $h\gtrless\overline{h}$; thus $h_c<\overline{h}$. That is, the rate of exponentiation h_c which contributes dominantly to the decay of the variance is less than the average rate $\overline{h}$.

To test this prediction we have made histograms of $P(h,t)$ from the orbits, from which we can determine $G(h)$, via

$$G(h)\simeq-\frac{1}{t}\ln(P(h,t)/t^{1/2}),$$

for large t. Figure 9 shows data points from the histogram along with a third order polynomial fit to $h+G(h)$. As discussed above the minimum of this function determines the decay rate. Note, as implied by the classical results in Ref. 5 and as observed in Ref. 4 this value is independent of the diffusion coefficient D. In particular, from the fit in Fig. 9 we obtain $\nu=1.91$ which compares favorably with the result at the full solution $\nu=1.87$.

Thus, we conclude that the long time decay of the scalar is determined by the eventual exponential growth in $k_{\swarrow}$ of a small number of orbits for which the initial k vector contains a small component of the exponentially growing solution. Further, the rate of exponentiation of the orbits which contribute the most, h_c, is less than the mean Lyapunov exponent $h_c<\overline{h}$. This long time behavior is likely to be strongly affected by the presence of KAM surfaces.

The exponential decay of the variance suggests that the scalar has formed an eigenfunction; termed a ''strange'' eigenfunction in Ref. 4. As further support for the eigenfunction picture we note that the various moments $\langle k^{\sigma}\rangle$ plotted in Fig. 6 are roughly independent of time during the long time exponential decay.

Figure 10 shows averages over time of the power spectrum $F(k,t)$ obtained from both the Fourier amplitude code and the orbit code. Figure 10(a) shows the result from the Fourier code averaged over two different time intervals $11\leqslant t/T\leqslant 20$ (solid curve) and $20\leqslant t/T\leqslant 30$ (dotted curve), where the vertical scale is normalized via

Downloaded¬10¬Jul¬2006¬to¬171.64.163.13.¬Redistribution¬subject¬to¬AIP¬license¬or¬copyright,¬see¬http://pof.aip.org/pof/copyright.jsp

$F(k,t)/\int dk F(k,t)$. The fact that the two curves in Fig. 10(a) coincide means that $F(k,t)$ assumes an asymptotically invariant k-dependence as it decays with time. Figure 10(b) shows results from the Fourier code (dotted) and the orbit code (solid) averaged over the time interval $20 \leqslant t \leqslant 30$. As can be seen, both codes predict essentially the same shape for the power spectrum.

We may obtain an analytic expression for the long time power spectrum as follows. We again use expression (18) for the power spectrum along with Eq. (21) for the time dependence of the elemental weights. We rewrite the exponent in Eq. (21) by multiplying and dividing by the final value of $k_{/\!/}^2(t)$

$$\omega_{/\!/}(t) = \omega_{/\!/}(0)\exp[-2Dk_{/\!/}^2(t)\tau_{/\!/}],$$

where

$$\tau_{/\!/} = \int_0^t dt' \frac{k_{/\!/}^2(t')}{k_{/\!/}^2(t)}.$$

As $k_{/\!/}$ grows exponentially with time the value of $\tau_{/\!/}$ is determined by the behavior of $k_{/\!/}(t')$ for t' within several exponentiation times of t. As the rate of exponentiation is not constant, one cannot simply replace $\tau_{/\!/}$ by $(2h_{/\!/})^{-1}$. We thus regard $\tau_{/\!/}$ and $h_{/\!/}$ as two distinct random variables; with $h_{/\!/}$ measuring the rate of exponentiation for the orbit averaged over a long time, $t \gg 1/h_{/\!/}$, and $\tau_{/\!/}$ measuring the rate of exponentiation over a short time in the recent past. As the distribution of h values is the same as is obtained by summing a large number of independent variables we argue that the values of $h_{/\!/}$ and $\tau_{/\!/}$ can be considered to be independent random variables. (The sum of a large number of random numbers depends weakly on any individual term in the sum.) Introducing probability distributions for $h_{/\!/}$ and $\tau_{/\!/}$ we replace the sum in Eq. (18) by integrations over h, τ, and the angle ϕ,

$$F(k,t) = \int \frac{d\phi}{2\pi} \int dh P(h,t) \int d\tau M(\tau)\delta[k - k_0|\cos\phi| \times \exp(ht)]\exp[-\tau k_0^2 D\cos^2\phi \exp(2ht)]$$

where $M(\tau)$ is the probability distribution for τ. Carrying out the integral over ϕ (expanding for $|\cos\phi| \ll 1$ as before) gives

$$F(k,t) = \frac{2}{\pi k_0} \int dh P(h,t)\exp(-ht) \int d\tau M(\tau)\exp(-\tau D k^2).$$

The integral over h gives the exponential decay dependence on time as before, while the k dependence of the power spectrum is determined by the distribution of τ values. That is,

$$F(k,t) \sim \exp(-\nu t)\overline{M}(\sqrt{D}k), \tag{24}$$

where

$$\overline{M}(s) = \int_0^\infty d\tau M(\tau)\exp[-s\tau] \tag{25}$$

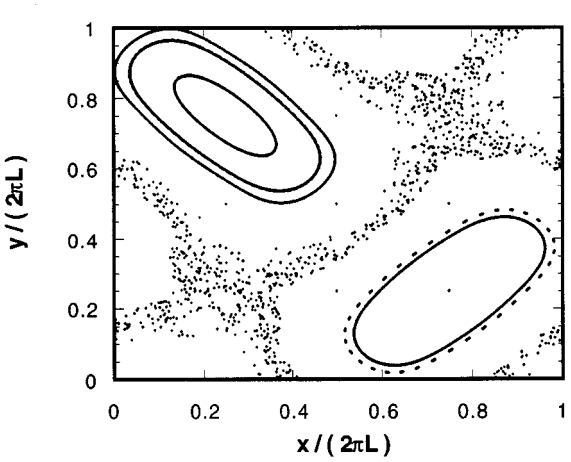

FIG. 11. Surface of section plot for a number of initial conditions with $\theta_1 = \theta_2 = 0$ and $UT/L = 0.5$.

is the Laplace transform of the probability distribution of τ. The width in k of the power spectrum thus scales with the diffusion coefficient as $D^{-1/2}$ while the decay rate is independent of D.

Equations (23) and (24) are the main results of this section. Equation (23) yields the exponential decay rate, while (24) states the factorization of the time dependence and gives an expression for the ''strange'' eigenfunction of Pierrehumbert. We emphasize that both ν and the function M (and $\overline{M}$) are determined purely by the dynamical behavior of fluid element trajectories and are consequently independent of D.

IV. TIME PERIODIC FLOW

In this section we will examine the power spectrum for cases in which the flow is time periodic, in particular, the angles θ_1 and θ_2 in Eq. (8) are set to zero. In this case only a fraction of the orbits are chaotic for the value of the magnitude of the flow velocity under consideration $e = UT/L = 0.5$. Surface of section plots for a number of initial conditions are shown in Fig. 11. As can be seen, most of phase space is integrable. Grey scale intensity plots of the scalar and gradient for this case are shown in Fig. 12. They

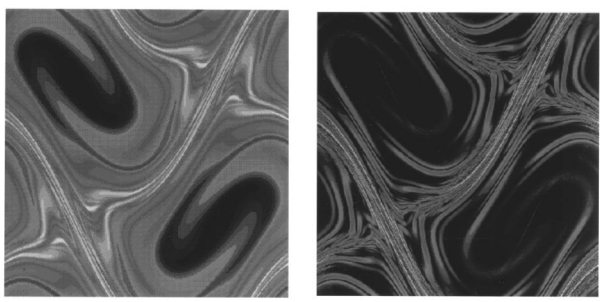

FIG. 12. Grey scale intensity plot of (a) the scalar and (b) the measure $\mu(s,t,1)$ defined in Eq. (19) for $t = 5T$, for the case $\theta_1 = \theta_2 = 0$, $UT/L = 0.5$.

Downloaded¬10¬Jul¬2006¬to¬171.64.163.13.¬Redistribution¬subject¬to¬AIP¬license¬or¬copyright,¬see¬http://pof.aip.org/pof/copyright.jsp

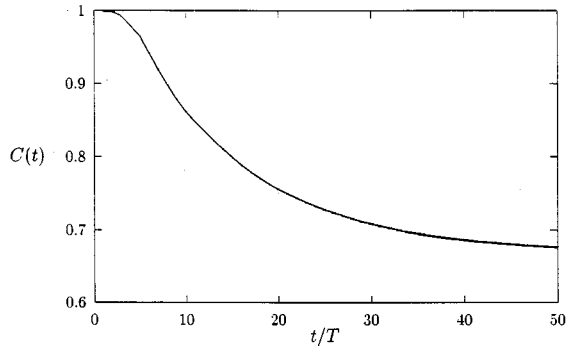

FIG. 13. The quantity $C(t)$ versus t/T in the case with no KAM surfaces present ($\theta_1=\theta_2=0$, $UT/L=0.5$) from the Fourier code.

are quite different than those in the fully chaotic case, Fig. 4.

A plot of $C(t)$ versus t obtained from the Fourier amplitude code for this case is shown in Fig. 13. There is an initial period in which the variance is constant corresponding to early times when diffusion is negligible. Subsequently the variance decays by about 30% and then becomes constant in time. This decrease is attributed to the decay of scalar variance in the chaotic regions of space where the growth of the wave vector is exponential. In the integrable region, nearby orbits do not diverge exponentially and the spectrum remains concentrated at low values of wave number. Ultimately this variance will decay due to diffusion but at a very low rate.

The above picture is confirmed by the behavior of the power spectrum with time shown in Fig. 14. The bulk of the variance remains at low k values while a portion, presumably corresponding to the chaotic orbits, ''cascades'' to high values of k where it is dissipated.

V. BATCHELOR'S LAW

According to Batchelor,[5] the power spectrum should depend inversely on k in the range of wave numbers greater than that of the flow but less than that where the variance is dissipated. Our previous work[2] argued that this behavior applied only for cases in which a source was present at low wave numbers, and the time asymptotic power spectrum was considered. Indeed, none of the simulation results shown so far in this paper conform to Batchelor's law. To recover Batchelor's law we show in Fig. 15 the asymptotic power spectrum $F_s(k)$ for the case in which the source is given by $S=\frac{1}{2}\cos[2\pi(x+y)/L]$. As can be seen the power spectrum has the proper k^{-1} dependence.

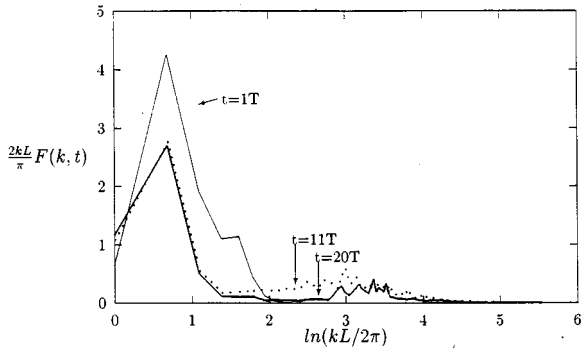

FIG. 14. The quantity $(2kL/\pi)F(k,t)$ versus $\ln(kL/2\pi)$ for the case with KAM surfaces from the Fourier code.

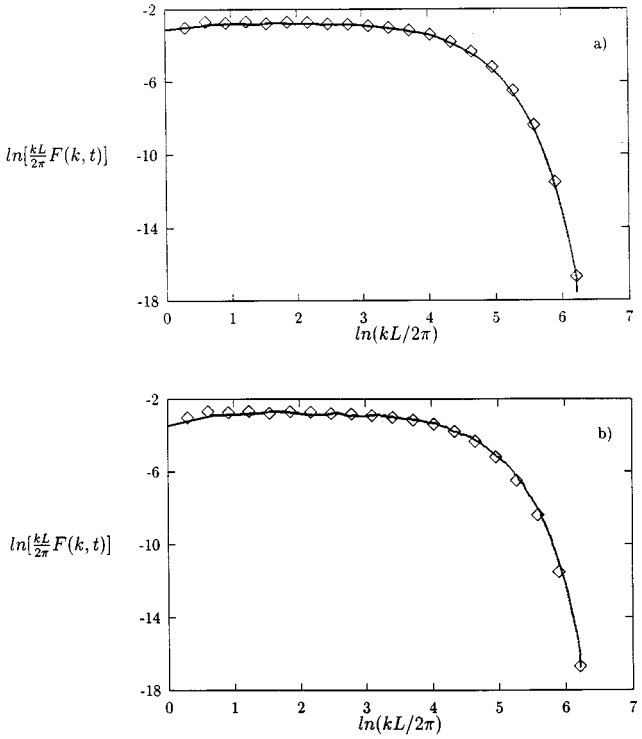

FIG. 15. (a) The quantity $\ln[(kL/2\pi)F_s(k)]$ versus $\ln(kL/2\pi)$ from the Fourier code (solid curve) and from the orbit code (diamonds) computed using a superposition of pulses. (b) The same quantities as in (a) except the solid curve is computed with a source rather than a superposition of pulses.

Our previous theory[2] argued that the ''steady state'' spectrum in the presence of a source (such as that shown in Fig. 15) could be obtained from a time integration of the transient spectra produced in the initial value case. Figure 15(a) shows this time integrated power spectrum as produced by both the Fourier amplitude code and the orbit code. Figure 15(b) compares the results of the Fourier code with a steady source with those of the orbit code using a time integration of the transient spectra. The major contribution to this time integration comes from the initial transient during which the power spectrum has the form of a pulse as shown in Fig. 2. As the rate of increase in the value of the wave number corresponding to the center of the pulse, k, is determined by the Lyapunov exponent, $dk/dt=hk$, the contribution of the moving pulse to the time average power spectrum is inversely proportional to k. This is the origin of Batchelor's law.

VI. CONCLUSIONS

We find that the reduced k-spectrum model provides a remarkably accurate description for the time evolution of the power spectrum of a passive scalar in a chaotic fluid flow. In this model, the power spectrum is determined by following

Downloaded¬10¬Jul¬2006¬to¬171.64.163.13.¬Redistribution¬subject¬to¬AIP¬license¬or¬copyright,¬see¬http://pof.aip.org/pof/copyright.jsp

an ensemble of fluid orbits associated with which are an ensemble of mean wave vectors and a contribution to the scalar variance. Since the reduced power spectrum is described in terms of the fluid orbits we can characterize the behavior of the power spectra using recently developed concepts in nonlinear dynamics. In particular a number of important features are related to the distribution of finite time Lyapunov exponents. These include the initial evolution of the power spectrum, its long time decay due to diffusion, and the form of the power spectrum in the presence of a source of scalar variance (Batchelor's law).

ACKNOWLEDGMENTS

This work was supported by the U.S. Department of Energy and by the Office of Naval Research (Physics).

APPENDIX: REDUCED *k*-SPECTRUM MODEL

In order to put our reduced k-spectrum model on firmer footing we rederive it here introducing the phase space action density $\tilde{N}(\mathbf{k},\mathbf{x},t)$ defined via

$$\tilde{N}(\mathbf{k},\mathbf{x},t)=\int d^n r \exp(-i\mathbf{k}\cdot\mathbf{r})\,\phi\left(\mathbf{x}+\frac{\mathbf{r}}{2}\right)\phi\left(\mathbf{x}-\frac{\mathbf{r}}{2}\right). \quad \text{(A1)}$$

We note that the transform of the correlation function $C(\mathbf{k},t)$ introduced in Eq. (5) is obtained by averaging the action density over space

$$\overline{C}(\mathbf{k},t)=\langle\tilde{N}(\mathbf{k},\mathbf{x},t)\rangle. \quad \text{(A2)}$$

Similarly, integration over wave vector k gives the local scalar variance

$$\phi^2(\mathbf{x})=\int \frac{d^n k}{(2\pi)^n}\tilde{N}(\mathbf{k},\mathbf{x},t). \quad \text{(A3)}$$

The definition of the action density (A1) may also be expressed in terms of the Fourier transform, $\phi(\mathbf{k},t)$ of the scalar, where

$$\phi(\mathbf{x},t)=\int \frac{d^n k}{(2\pi)^n}\overline{\phi}(\mathbf{k},t)e^{i\mathbf{k}\cdot\mathbf{x}},$$

namely,

$$\tilde{N}(\mathbf{k},\mathbf{x},t)=\int \frac{d^n q}{(2\pi)^n}e^{i\mathbf{q}\cdot\mathbf{x}}\overline{\phi}\left(\mathbf{k}+\frac{1}{2}\mathbf{q},t\right)\overline{\phi}^*\left(\mathbf{k}-\frac{1}{2}\mathbf{q},t\right). \quad \text{(A4)}$$

We now derive an evolution equation for the action density from Eq. (1). Specifically we form

$$\frac{\partial\tilde{N}(\mathbf{k},\mathbf{x},t)}{\partial t}=\int d^n r\ \exp(-i\mathbf{k}\cdot\mathbf{r})\left[\phi\left(\mathbf{x}+\frac{\mathbf{r}}{2}\right)\frac{\partial}{\partial t}\phi\left(\mathbf{x}-\frac{\mathbf{r}}{2}\right)+\phi\left(\mathbf{x}-\frac{\mathbf{r}}{2}\right)\frac{\partial}{\partial t}\phi\left(\mathbf{x}+\frac{\mathbf{r}}{2}\right)\right],$$

and use Eq. (1) to replace the time derivatives of ϕ. To evaluate these terms it is useful to first express quantities in terms of their Fourier transforms and then to utilize Eq. (A4). The result is

$$\frac{\partial}{\partial t}\tilde{N}+\boldsymbol{\nabla}\cdot\int\frac{d^n q}{(2\pi)^n}\overline{\mathbf{v}}(\mathbf{q},t)e^{i\mathbf{q}\cdot\mathbf{x}}\frac{1}{2}\left(\tilde{N}\left(\mathbf{k}-\frac{\mathbf{q}}{2}\right)+\tilde{N}\left(\mathbf{k}+\frac{\mathbf{q}ht}{2}\right)\right)+i\mathbf{k}\cdot\int\frac{d^n q}{(2\pi)^n}\overline{\mathbf{v}}(\mathbf{q},t)e^{i\mathbf{q}\cdot\mathbf{x}}\left(\tilde{N}\left(\mathbf{k}-\frac{\mathbf{q}}{2}\right)-\tilde{N}\left(\mathbf{k}+\frac{\mathbf{q}}{2}\right)\right)=2D\left[\frac{1}{4}\nabla^2-k^2\right]\tilde{N}(\mathbf{k},\mathbf{x},t), \quad \text{(A5)}$$

where $\overline{\mathbf{v}}(\mathbf{q},t)$ is the spatial Fourier transform of the flow $\mathbf{v}(\mathbf{x},t)$.

So far, Eq. (A5) is exact. At this point we make the assumption that $\tilde{N}(\mathbf{k},\mathbf{x},t)$ extends to high values of $|\mathbf{k}|$ compared with the characteristic wave number of the flow. Further, we focus on the smoothly varying in phase space part of $\tilde{N}(\mathbf{k},\mathbf{x},t)$ which we label $N(\mathbf{k},\mathbf{x},t)$. These assumptions allow us to Taylor expand the q dependence of $\tilde{N}(\mathbf{k}\pm\mathbf{q}/2)$ on the left hand side of Eq. (A5) and to drop the Laplacian on the right hand side compared with k^2. The result is

$$\frac{\partial}{\partial t}N(\mathbf{k},\mathbf{x},t)+\boldsymbol{\nabla}\cdot(\mathbf{v}(\mathbf{x},t)N(\mathbf{k},\mathbf{x},t))-\nabla\mathbf{v}(\mathbf{x},t)\cdot\mathbf{k}\cdot\frac{\partial}{\partial\mathbf{k}}N(\mathbf{k},\mathbf{x},t)=-2k^2DN. \quad \text{(A6)}$$

For the case in which the flow is incompressible in space (A6) is the wave kinetic equation for disturbances with dispersion relation $\omega=\mathbf{k}\cdot\mathbf{v}$. The characteristics are then given by Hamilton's equation

$$\frac{d\mathbf{x}}{dt}=\frac{\partial\omega}{\partial\mathbf{k}}=\mathbf{v}(\mathbf{x},t),$$

$$\frac{d\mathbf{k}}{dt}=-\frac{\partial\omega}{\partial\mathbf{x}}=-\boldsymbol{\nabla}\mathbf{v}\cdot\mathbf{k}.$$

The general solution for the smoothed action density can then be expressed in terms of the phase space trajectories $\boldsymbol{\xi}(\mathbf{x}',t)$ and $\boldsymbol{\kappa}(\mathbf{x}',\mathbf{k}',t)$ where $d\boldsymbol{\xi}/dt=\mathbf{v}(\boldsymbol{\xi},t)$, $d\boldsymbol{\kappa}/dt=-\boldsymbol{\nabla}\mathbf{v}(\boldsymbol{\xi},t)\cdot\boldsymbol{\kappa}$, and $\boldsymbol{\xi}(\mathbf{x}',0)=\mathbf{x}'$, $\boldsymbol{\kappa}(\mathbf{x}',\mathbf{k}',0)=\mathbf{k}'$. The result is

$$N(\mathbf{x},\mathbf{k},t)=\int d^n x' d^n k' N(\mathbf{x}',\mathbf{k}',0)\,\delta(\mathbf{x}-\boldsymbol{\xi}(\mathbf{x}',t))\times\delta(\mathbf{k}-\boldsymbol{\kappa}(\mathbf{x}',\mathbf{k}',t))\exp\left[-2D\int_0^t\kappa^2 dt'\right].$$

Our model corresponds to the above solution in the case in which the continuous integrations over the initial phase space coordinates are replaced by a discrete sum over initial conditions. Using Eqs. (A2) and (4) we then obtain (18). Equation (A6) can be viewed as a WKB (Wentzel, Kramers, and Brillouin) type description of the passive scalar. Similar formulations have been applied recently with success[12] to other problems in fluid mechanics.

[1]Some recent works on the convection of passive scalars in flow fields are the following: H. Aref, ''Stirring by chaotic advection,'' Fluid Mech. **143**, 1 (1984); T. Dombre, U. Frisch, J. M. Greene, M. Henon, A. Mehr, and A. M. Soward, ''Chaotic streamlines in the ABC flow,'' *ibid.* **167**, 353 (1986); J. Chaiken, C. K. Chu, M. Tabor, and Q. M. Tran, ''Lagrangian turbulence and spatial complexity in a stochastic flow,'' Phys. Fluids **30**, 687 (1987); D. V. Khakhar, H. Rising, and J. M. Ottino, ''Analysis of chaotic mixing in two model systems,'' J. Fluid Mech. **172**, 419 (1986); S.

Downloaded¬10¬Jul¬2006¬to¬171.64.163.13.¬Redistribution¬subject¬to¬AIP¬license¬or¬copyright,¬see¬http://pof.aip.org/pof/copyright.jsp

W. Jones and H. Aref, ''Chaotic advection in pulsed source-sink systems,'' Phys. Fluids **31**, 469 (1988); T. H. Solomon and J. P. Gollub, ''Passive transport in steady Rayleigh–Bénard convection,'' *ibid*. **31**, 1372 (1988); F. Heslot, B. Castaing, and A. Libshaber, ''Transition to turbulence in helium gas,'' Phys. Rev. A **36**, 5870 (1987); B. Castaing, G. Gunaratne, F. Heslot, L. Kadanoff, A. Libshaber, S. Thomas, X. Z. Wu, S. Zaleski, and G. Zanetti, ''Scaling of hard thermal turbulence in Rayleigh–Bénard convection,'' J. Fluid Mech. **204**, 1 (1989); Ya. G. Sinai and V. Yakhot, ''Limiting probability distributions of a passive scalar in a random velocity field,'' Phys. Rev. Lett. **63**, 1962 (1989); H. Chen, S. Chen, and R. H. Kraichnan, ''Probability distribution of a stochastically convected scalar field,'' *ibid*. **63**, 2657 (1989); A. Crisanti, M. Falcioni, G. Paladin, and A. Vulpiani, ''Role of Lagrangian chaoticity on the small scale structure of passive scalars in fluids,'' Physica A **166**, 305 (1990); R. Ramshakar and J. Gollub, ''Transport by capillary waves, Part II: Scalar dispersion and structure of the concentration field,'' Phys. Fluids A **3**, 1344 (1991); A. Majda, ''The random uniform shear layer: An explicit example of turbulent diffusion with broad tail probability distributions,'' *ibid*. **5**, 1963 (1993); B. Shraiman and E. Siggia, ''Lagrangian path integrals and fluctuations in random flow,'' Phys. Rev. E **49**, 2912 (1994).

[2]T. M. Antonsen, Jr. and E. Ott, ''Multifractal power spectra of passive scalars convected by chaotic fluid flows,'' Phys. Rev. A **44**, 851 (1991).

[3]E. Ott and T. M. Antonsen, Jr. ''Fractal measures of passively convected vector fields and scalar gradients in chaotic fluid flows,'' Phys. Rev. A **39**, 3660 (1989); ''Chaotic fluid convection and the fractal nature of passive scalar gradients,'' Phys. Rev. Lett. **61**, 2839 (1988).

[4]R. Pierrehumbert, ''On tracer microstructure in the large-eddy dominated regime,'' Chaos, Solitons Fractals **4**, 1091 (1994).

[5]A. M. Obukov, ''Structure of the temperature field in turbulent flow,'' Izv. Akad. Nauk. Geogr. Geofiz. **13**, 58 (1949); S. Corrsin, ''On the spectrum of isotropic temperature fluctuations in an isotropic turbulence,'' J. Appl. Phys. **22**, 469 (1951); G. K. Batchelor, ''Small-scale variation of convected quantities like temperature in a turbulent fluid. Part I,'' J. Fluid Mech. **5**, 113 (1959); R. H. Kraichnan, ''Small-scale structure of a scalar field convected by turbulence,'' Phys. Fluids **11**, 945 (1968); R. H. Kraichnan, ''Convection of a passive scalar by a quasi-uniform random stirring field,'' J. Fluid Mech. **64**, 737 (1974).

[6]R. R. Prasad, C. Meneveau, and K. R. Sreenivasan, ''Multifractal nature of the dissipation field of passive scalars in fully developed turbulence,'' Phys. Rev. Lett. **61**, 74 (1988). See this paper for additional relevant references on experiments in turbulent fluids.

[7]P. Grassberger, R. Badii, and A. Politi, ''Scaling laws for invariant measures on hyperbolic and nonhyperbolic attractors,'' J. Stat. Phys. **51**, 135 (1988); H. Hata, T. Horita, H. Mori, T. Morita, and K. Tomita, ''Characterization of local structures of chaotic attractors in terms of coarse-grained local expansion rates,'' Prog. Theor. Phys. **80**, 809 (1988); E. Ott, C. Grebogi, and J. A. Yorke, ''Theory of first order phase transitions for chaotic attractors of nonlinear dynamical systems,'' Phys. Lett. **135A**, 343 (1989).

[8]M. A. Sepulveda, R. Badii, and E. Pollak, ''Spectral analysis of conservative dynamical systems,'' Phys. Rev. Lett. **63**, 1226 (1989).

[9]T. Horita, H. Hata, R. Ishizaki, and H. Mori, ''Long-time correlations and expansion rate spectra of chaos in Hamiltonian systems,'' Prog. Theor. Phys. B **3**, 1065 (1990).

[10]F. Varosi, T. M. Antonsen, Jr., and E. Ott, ''The spectrum of fractal dimensions of passively convected scalar gradients in chaotic fluid flows,'' Phys. Fluids A **3**, 1017 (1991).

[11]F. J. Muzzio, P. D. Swanson, and J. M. Ottino, ''The statistics of stretching and stirring in chaotic flows,'' Phys. Fluids A **3**, 822 (1991); F. J. Muzzio, C. Meneveau, P. D. Swanson, and J. M. Ottino, ''Scaling and multifractal properties of mixing in chaotic fluids,'' Phys. Fluids A **4**, 1439 (1992).

[12]S. Friedlander and M. Vishik, ''Dynamo theory, vorticity generation, and exponential stretching,'' Chaos **1**, 198 (1991); A. Lifshitz and E. Hameiri, ''Local stability conditions in fluid dynamics,'' Phys. Fluids A **3**, 2644 (1991).

Downloaded¬10¬Jul¬2006¬to¬171.64.163.13.¬Redistribution¬subject¬to¬AIP¬license¬or¬copyright,¬see¬http://pof.aip.org/pof/copyright.jsp